ACS OMEGA

http://pubs.acs.org/journal/acsodf

Article

Novel Porous Rhodium Metal−Organic Aerogel for Efficient Removal of Organic Dyes and Catalysis of Si−H Insertion Reactions

Hong-Guang Fu* and Jinmao You*

Cite This: *ACS Omega* 2021, 6, 26766−26772

Read Online

ACCESS | Metrics & More | Article Recommendations | Supporting Information

ABSTRACT: Metal−organic gels (MOGs) are attracting increasing attention for removal of organic dyes from aqueous solution and for catalysis of Si−H insertion reactions. Herein, we report that a reaction of porphyrin derivative **1** with $Rh_2(OAc)_4$ generates stable metal−organic gels and subsequent subcritical carbon dioxide drying affords metal−organic aerogels. Owing to their micro- and mesoporosity, the aerogels adsorbed dyes. Moreover, aerogel I catalyzed Si−H insertion reactions to give organosilicon compounds in high yields.

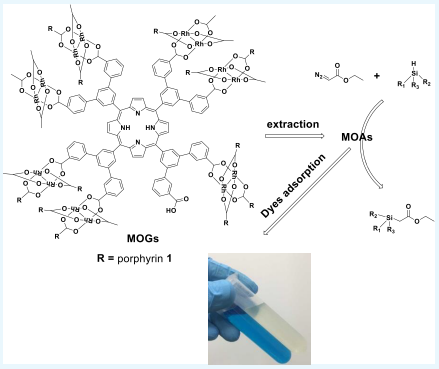

INTRODUCTION

Pollution of water by organic contaminants such as dyes and pharmaceuticals poses a potential threat to human health and the environment.[1] Because these contaminants can float on the water surface, they can reduce light penetration into the water,[2] thus hindering photosynthesis by phytoplankton; more importantly, some of these compounds are toxic and even carcinogenic to organisms.[3] Several techniques have been used for organic dye removal, including photocatalytic degradation,[4] membrane filtration,[5] electrolysis,[6] and adsorption.[7] Of these techniques, adsorption is considered as the most promising because of its low cost and operational simplicity.[8] Adsorbents used for this purpose include activated carbon, polymer gels, natural biomass, inorganic nanomaterials, and metal−organic frameworks (MOFs).[9] However, the currently available adsorbents have some deficiencies, such as slow pollutant uptake, poor removal capacity, high energy consumption, and low thermal, physical, and chemical resistance, which decrease the removal performance of these adsorbents.[10] Hence, the development of adsorbents with high adsorption capacity, rapid removal rate, excellent selectivity, and reusability would be highly desirable.[11] Some research studies have already been done in this area. For example, Park and co-workers reported a novel route for the synthesis of porous titanium−porphyrinic gels that have tunable surface areas and rapidly adsorb bulky dyes under ambient conditions.[12]

Compared with other nanostructured porous materials such as covalent−organic frameworks,[13] MOFs exhibit distinctive chemical versatility, unprecedented thermal stability, and ultrahigh specific surface areas,[14] and they have been shown to have fascinating applications in sensors, catalysis, drug delivery, gas adsorption and separation, and dye adsorption.[15] The only disadvantage of MOFs is that they are usually obtained in a powder form, and methods for molding them into bulk forms or particles are urgently needed if they are to find practical applications for adsorption and catalysis. However, molding requires the addition of adhesives, which reduces the surface area of MOFs.[16]

Metal−organic gels (MOGs) are a class of porous material that has emerged as alternatives to MOFs. MOGs are assembled from bridging metal ions and organic ligands and have features that differ from those of supramolecular gels held together by common noncovalent interactions.[17] Unlike MOFs, MOGs show poor crystallinity, and their exact structures remain undetermined.[18] In MOGs, a coordination process will be cross-linked in the form of primary particles and randomly cross−linked into the reaction system to form a three-dimensional porous network in which solvent molecules are trapped.[19] Thus, unlike common supramolecular gels, most MOGs fail to undergo an irreversible sol−gel transition under the influence of external stimuli.[20] In addition, removal of solvent from MOGs by means of supercritical CO_2 drying can result in the formation of metal−organic aerogels (MOAs), which have ultralow density, preserved porosity, and micro-, meso-, and macro-pores.[21] For example, the MOA of AlBDC-3:2-0.15 fabricated

Received: August 9, 2021
Accepted: September 16, 2021
Published: September 28, 2021

ACS Publications

© 2021 The Authors. Published by American Chemical Society

https://doi.org/10.1021/acsomega.1c04265
ACS Omega 2021, 6, 26766−26772

Scheme 1. Synthesis of Metal−Organic Aerogels from the Free Base of Porphyrin 1 and Dirhodium(II) Tetraacetate ($Rh_2(OAc)_4$)

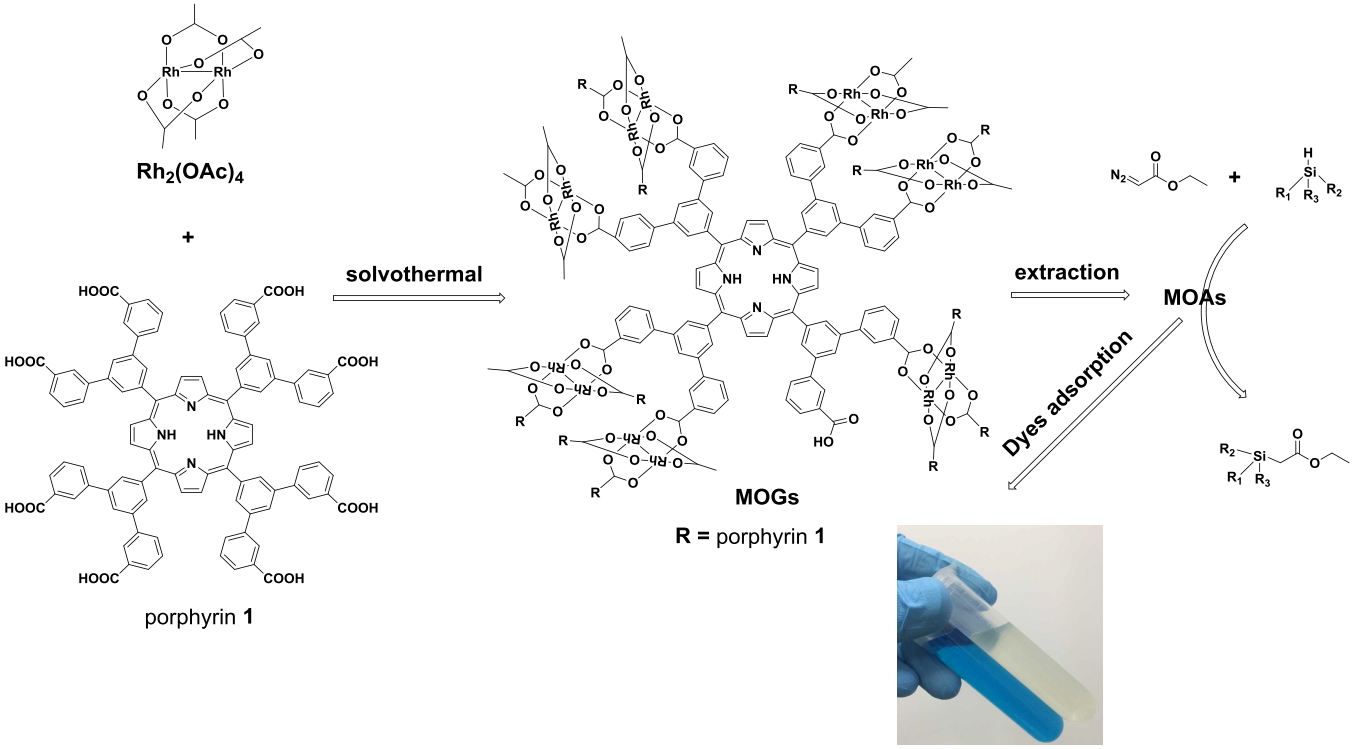

by Su *et al.*[22] exhibited a density of 0.299 g cm^{-3}, which is close to the values of the lightest MOFs (0.291 of NU-100[23] and 0.25 of MOF-210[24]). Owing to the aforementioned properties, MOAs have found applications as adsorbents and catalysts. On the other hand, porphyrins are good macrocyclic building blocks with rich coordination chemistry, and porphyrins with various peripheral substituents have been widely used for construction of porous materials.[25]

Transition-metal-catalyzed insertion of carbenes into Si−H bonds, a reaction that was initially reported by Doyle *et al.*,[26] has recently been used to construct organosilicon compounds. These carbene insertion reactions can generate new C−Si bonds in a single step and have found a broad array of applications in organic synthesis, agricultural chemistry, materials science, and pharmaceutical chemistry.[27] This method has several potential advantages: (1) the operation process is simple, (2) the reaction conditions are mild, and (3) these methods can achieve high enantioselective synthesis and atom economy of some chiral organosilanes that are difficult to obtain by means of traditional methods. In addition to iridium and ruthenium complexes, which are by far the most general catalysts for this purpose, dirhodium(II) complexes have also garnered considerable attention as catalysts for Si−H insertion reactions. In these complexes, the bridging of the two rhodium centers by four ligands results in the formation of a paddle-wheel structure in which two axial positions of the metal ions remain uncoordinated and can act as active catalytic sites.[28] However, most of the reported dirhodium(II)-catalyzed processes have been carried out in homogeneous solution to ensure sufficient contact between substrates and catalysts, and thus the practical utility of the complexes is limited. To our knowledge, there have been only a few studies on heterogeneous dirhodium(II)-catalyzed Si−H insertion reactions that occur under mild conditions.

RESULTS AND DISCUSSION

In the current study, we designed and fabricated a series of black MOGs by means of reactions between the free base of porphyrin **1** and dirhodium(II) tetraacetate ($Rh_2(OAc)_4$) followed by extraction with supercritical CO_2 to obtain MOAs; this method effectively prevented the collapse of the porous structures upon extraction (Scheme 1). In addition, we thoroughly studied the effects of precursor concentration, **1**/$Rh_2(OAc)_4$ molar ratio, and solvent on MOG formation. The obtained MOAs displayed high thermal stability and Brunauer−Emmett−Teller surface areas, as indicated by thermogravimetric analysis and N_2 adsorption isotherms at 77 K, respectively. Intriguingly, one of the MOAs could adsorb hazardous organic dyes from water. Moreover, owing to its permeable three-dimensional network and the presence of the two rhodium atoms, the same MOA also catalyzed Si−H insertion reactions to afford organosilicon compounds at room temperature.

The creation of a three-dimensional network requires that both the linker and metal have a connectivity of >2. Therefore, we designed porphyrin **1**, which bears eight carboxylic acid groups and can thus form gels with eight binding sites upon the reaction with $Rh_2(OAc)_4$. Porphyrin **1** was synthesized via a condensation reaction between pyrrole and **2** followed by hydrolysis of the esters in the resulting intermediate with aqueous KOH. The details of the synthesis and the characterization data for **1** are provided in the Supporting Information (Scheme S1 and Figures S1−S4).

The reaction between **1** and $Rh_2(OAc)_4$ in various solvent mixtures (DMF/H_2O, DMF/MeOH, and DMF/EtOH) at molar ratios of 1:2, 1:1, 2:1, and 3:1 at 85 °C for 72 h gave black MOGs (Table 1). When 10:1 (v/v) DMF/H_2O was used as the solvent, the **1**/$Rh_2(OAc)_4$ molar ratio and the reactant concentrations did not affect the formation of gels (entries 1−

https://doi.org/10.1021/acsomega.1c04265
ACS Omega 2021, 6, 26766−26772

Table 1. Effects of Reactant Concentration, Solvent, and Ligand/Metal Ratio on Gelation of 1 and $Rh_2(OAc)_4$

entry	1:M[a]	1 (mmol)	M (mmol)	solvent[b]	result	designation
1	1:2	0.015	0.03	DMF/H_2O = 10:1	gel	A
2	1:2	0.0075	0.015	DMF/H_2O = 10:1	gel	B
3	1:1	0.0075	0.0075	DMF/H_2O = 10:1	gel	C
4	2:1	0.0075	0.00375	DMF/H_2O = 10:1	gel	D
5	3:1	0.0075	0.0025	DMF/H_2O = 10:1	gel	E
6	1:2	0.015	0.03	DMF/MeOH = 1:1	no gel	F[c]
7	1:2	0.015	0.03	DMF/H_2O = 1:1	no gel	G[c]
8	1:2	0.015	0.03	DMF/MeOH = 10:1	gel	H
9	1:2	0.015	0.03	DMF/EtOH = 1:1	gel	I
10	1:2	0.015	0.03	DMF/EtOH = 10:1	gel	J

[a]M = $Rh_2(OAc)_4$. [b]The total volume of solvent was 2.2 mL. [c]F and G are powder.

5). However, when 1:1 DMF/H_2O was used as the solvent and the **1**/$Rh_2(OAc)_4$ ratio was 1:2, no gel formed (entry 7). Using a 1:2 **1**/$Rh_2(OAc)_4$ molar ratio, we tested a DMF/MeOH solvent system, which gave results similar to the DMF/H_2O system (compare entries 6 with 8). Interestingly, when EtOH was used instead of MeOH, gel formation occurred regardless of whether the DMF/EtOH ratio was 10:1 or 1:1 (entries 9 and 10). We also investigated the effect of the ligand/metal molar ratio and found that the ideal **1**/$Rh_2(OAc)_4$ ratio was 1:2 (compare entries 2−4) because the −COOH/dirhodium molar ratio was 4:1. Note that the gelation state of the MOGs was evaluated by turning the gelatinization reaction tube upside down (Figure S5, Supporting Information).

We subjected the MOGs to thorough solvent exchange with fresh EtOH (10 times each over the course of 3 days) to remove the excess reaction solvent and precursors; we chose EtOH because it is miscible with subcritical CO_2(l), which was subsequently used to dry the gels. The wet MOGs were dried with subcritical CO_2(l) to generate the corresponding MOAs, a process that resulted in minimal changes to the original structures. The Fourier transform infrared spectrum of free porphyrin **1** showed a stretching band for the —C(═O)— of the carboxylate groups at 1696 cm^{-1}, whereas MOA I showed a characteristic Ar−COO− asymmetrical stretching band at around 1560 cm^{-1}; this approximately 136 cm^{-1} red shift confirmed the coordination reaction between **1** and $Rh_2(OAc)_4$ (Figure S6, Supporting Information). In addition, the spectrum of MOA I also had a band at around 1696 cm^{-1}, implying that the aerogel formation reaction was incomplete.

Thermogravimetric analysis was used to study the thermostability of the aerogels (Figure S7, Supporting Information). Aerogel I showed a small total weight loss of 11% at a temperature below approximately 185 °C, corresponding to the release of solvents from inside the pores and from the surface. At above 185 °C, an abrupt weight loss was observed, indicating substantial decomposition of the gel's coordination network. That is, MOA I showed good thermal stability up to ∼185 °C.

To investigate the spatial structures of the MOAs, we carried out powder X-ray diffraction analysis of MOA I (Figure S8, Supporting Information). A representative curve for I exhibited only one broad peak, at a 2θ value of 4.0−24.1°, demonstrating

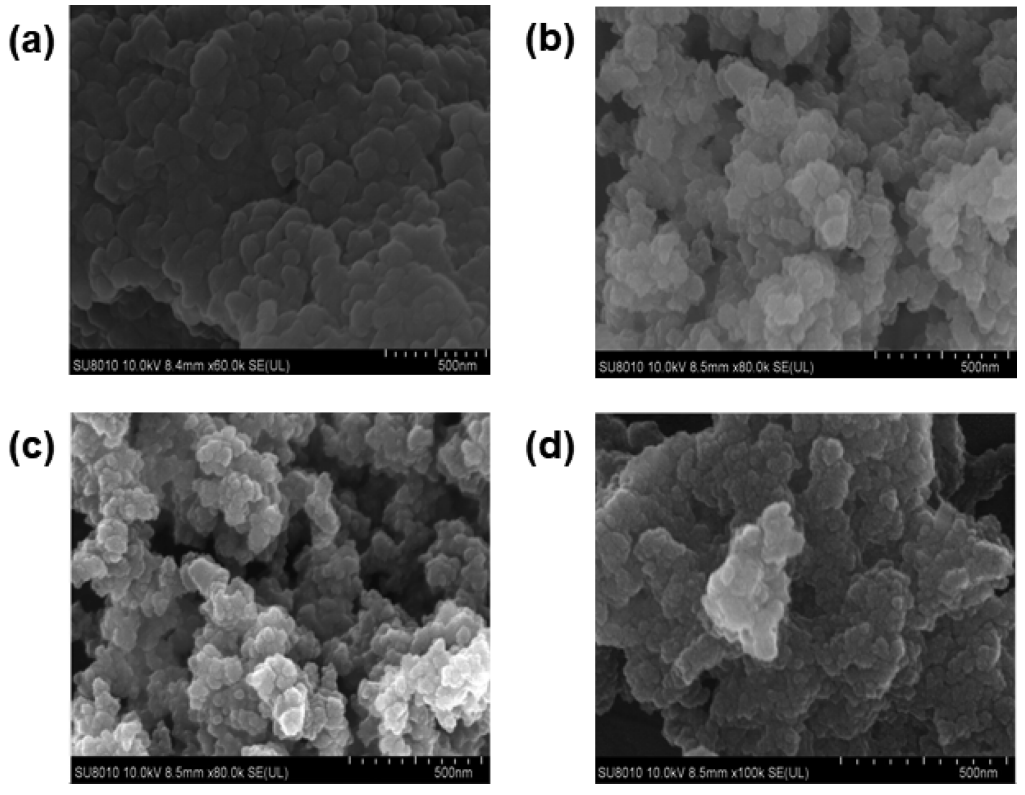

Figure 1. Scanning electron microscopy images of MOAs (a) A, (b) D, (c) I, and (d) J.

https://doi.org/10.1021/acsomega.1c04265
ACS Omega 2021, 6, 26766−26772

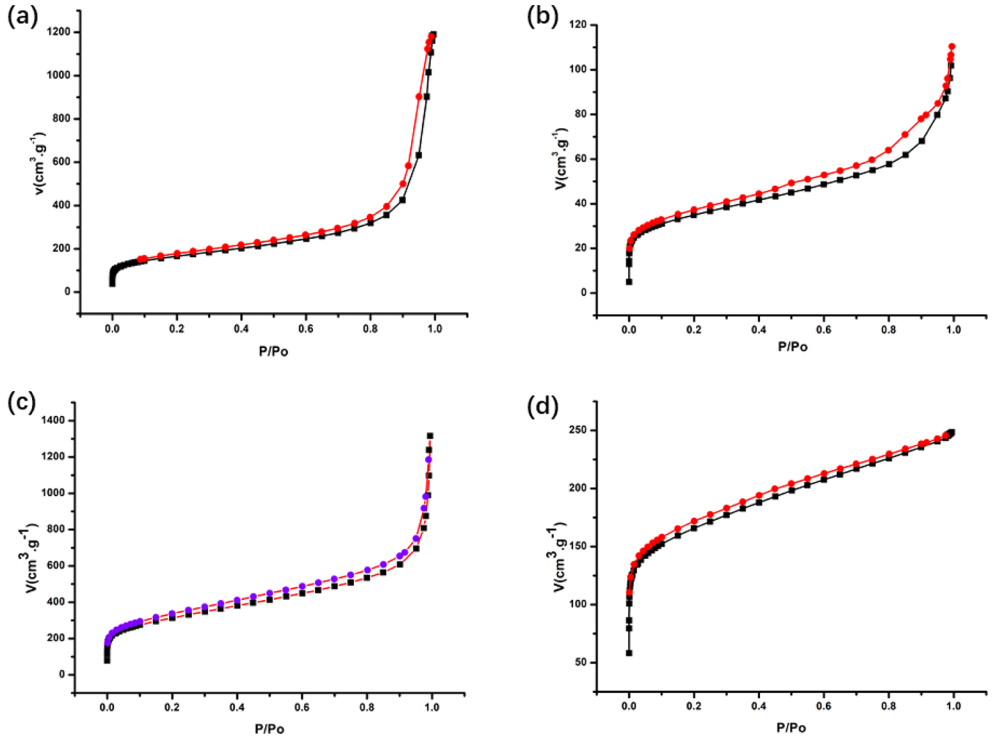

Figure 2. N_2 adsorption−desorption isotherms of MOAs (a) A, (b) D, (c) I, and (d) J.

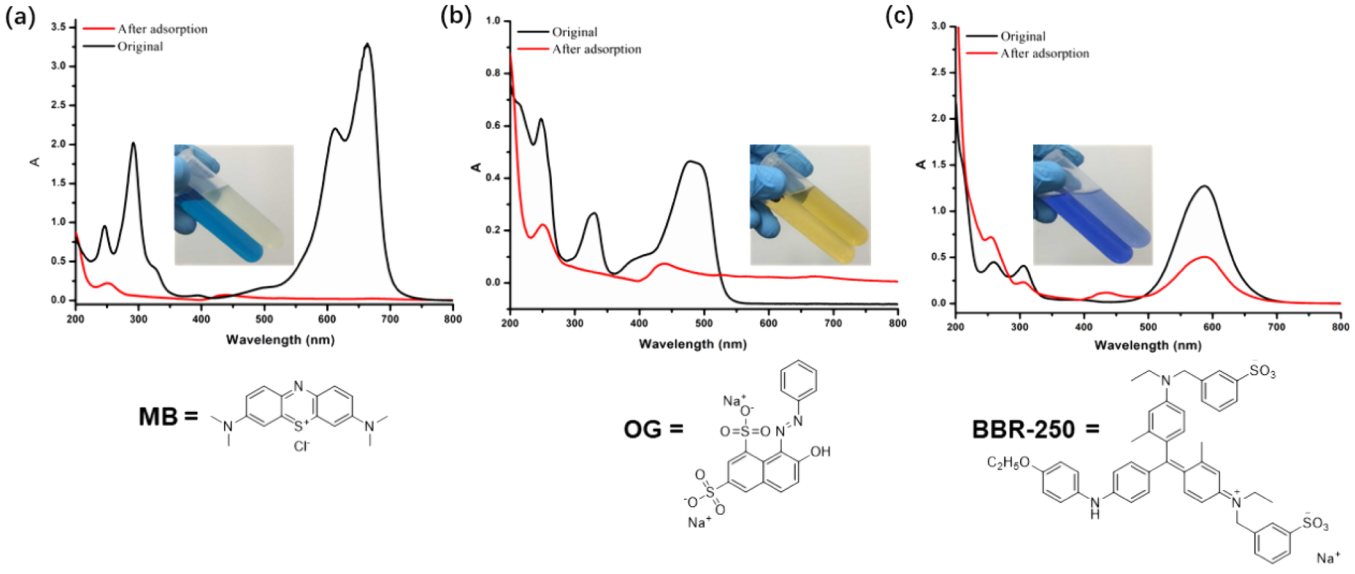

Figure 3. UV−vis absorption spectra showing uptake of organic dyes (a) MB, (b) OG, and (c) BBR-250 by MOA I. The insets show photographs of the dye solutions before and after adsorption.

that this MOA had an amorphous structure lacking a long-range order. Scanning electron microscopy was used to observe the surface morphology of the obtained gels (Figure 1). All the MOAs clearly had sponge-like porous networked structures consisting of interconnected spherical nanoparticles. Moreover, scanning electron microscopy reveals that macro- and mesopores were distributed throughout the gel network and that the pores of MOA I were bigger and more obvious than those of the other MOAs.

The permanent porosities of the obtained MOAs were determined by means of nitrogen physisorption at 77 K (Figure 2). The porosities were affected by various parameters, including the solvent in which they were prepared and the metal/ligand ratio. Prior to the physisorption measurements, the MOAs were degassed at 85 °C for 12 h under a vacuum. MOAs A and I showed typical type-IV adsorption isotherms, according to the IUPAC classification. In contrast, MOA D showed type-II adsorption behavior, and the isotherm of MOA J was type-I. On the basis of the abrupt-onset adsorption at low pressure, we concluded that both micro- and mesopores were present in the MOAs (Figure S9, Supporting Information). In all the measured MOAs, I had the highest Brunauer−Emmett−Teller surface area at 1124.3 $m^2\ g^{-1}$; the values for MOAs A, D, and J were 591.8, 125.5, and 605.3 $m^2\ g^{-1}$, respectively (Table S1,

https://doi.org/10.1021/acsomega.1c04265
ACS Omega 2021, 6, 26766−26772

Supporting Information). The micropores of all the MOAs had diameters of approximately 0.9 nm (Table S1, Supporting Information). On the basis of the scanning electron microscopy images and N_2 adsorption tests, MOA I was selected for additional studies.

To further evaluate the adsorption properties of the MOAs, we selected organic dyes with various charges for pollutant uptake tests. MOA I (8.00 mg) was added to 8 mL of a 20 mg L^{-1} aqueous solution of dye (cationic dye methylene blue [MB] = 14.4 × 6.1 Å^2, anionic dye Orange G [OG] = 15.6 × 10.1 Å^2, or anionic dye Coomassie brilliant blue G-250 [BBR-250] = 22.0 × 18.0 Å^2), and the UV−vis spectra of the resulting solutions were measured (Figure 3). In all the dyes, MB was adsorbed with the highest efficiency; the absorption intensity of the solution decreased by approximately 99.5% after 60 min, and the solution changed from dark blue to colorless. MOA I showed a moderate ability to adsorb OG (the removal efficiency was 89%), and the dye solution changed from slightly yellow to deep yellow, a change that could be attributed to the partial dissolution of the ligands. In contrast, MOA I failed to adsorb BBR-250 efficiently; the intensity of its characteristic peaks decreased by only 60%. The capability of MOA I to host a dye molecule (MB) with the approximate dimension suggested that MOA I may have an ability to absorb sizes matching substrates and product molecules in catalytic reactions, providing a possibility to serve as a catalyst.

The ability of the MOAs to catalyze the reaction of triethylsilane and ethyl diazoacetate was evaluated (Scheme 2). Of the tested MOAs, I, A, D, and J showed the best

Scheme 2. Chemical Equation of the MOA-Catalyzed Si−H Insertion Reaction of Triethylsilane and Ethyl Diazoacetate

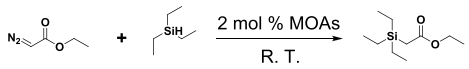

conversion rates (Table S2, Supporting Information, entries 1, 2, 5, and 8). However, the reaction times for A and D were much longer than those for I and J. Of the latter two MOAs, I showed the best performance. However, we were surprised to find that MOA I showed no catalytic activity for the reactions of primary or secondary silanes.

MOA I could be used to catalyze the reactions of tertiary silanes other than triethylsilane to give the corresponding Si−H insertion products, with varying reaction times and conversion rates (Table S3, Supporting Information). As the molecular volume of silane increased, the reaction time gradually increased and the conversion rate decreased. In addition, by comparing entries 1 with 2 in Table S3, the electron-donating groups can play a positive role in the Si-−H insertion reaction. These trends can be explained by the synergy of electronic effects and the fact that silanes with smaller molecular volumes could more readily enter the pores of the gel and bind to the rhodium sites that catalyzed the Si−H insertion reaction. Pleasantly, the MOA I can be isolated easily by centrifugation and reused for more than five runs with little loss of its catalytic activity (Figure S10, Supporting Information).

CONCLUSIONS

In conclusion, we fabricated a series of novel porphyrin−dirhodium(II) MOGs from porphyrin **1** and $Rh_2(OAc)_4$ and converted them to the corresponding MOAs by drying them with subcritical CO_2(l). The MOAs had large pore volumes and high specific surface areas, as indicated by N_2 adsorption experiments at 77 K. The MOAs show ana excellent performance for adsorption of dyes, including the hazardous dye MB. In addition, the MOAs catalyzed the Si−H insertion reaction between tertiary silanes and diazo compounds.

EXPERIMENTAL SECTION

Materials and Methods. All the reagents and solvents were commercially available and used as received unless otherwise their purification is specified. Compound **2**[29] was prepared according to the literature procedure with little modification. Column chromatography was performed on 200−300 mesh silica gel. Infrared spectra on KBr pellets were collected with a Nicolet/Nexus-670 FT−IR spectrometer in the region of 350−500 cm^{-1}. Scanning electron microscopy (SEM) was performed using a Quanta 400F scanning electron microscope. Before measurement, the aerogel sample was dispersed in ethanol with the aid of sonication, placed on aluminum foil, and sputter-coated with gold. The ^{1}H nuclear magnetic resonance (^{1}H NMR) spectra were recorded on a Bruker AVANCE III 400 MHz system (400 MHz). Powder X-ray diffraction patterns (PXRD) were collected on a Japan Rigaku X-ray diffractometer. Thermogravimetric analyses were performed under a N_2 atmosphere with a NETZSCH TG STA 449 F3 Jupiter system. UV/vis spectra were measured on a Shimadzu-2450 spectrophotometer. Gas adsorption measurements were carried out using a Quantachrome Autosorb-iQ2 analyzer. Prior to an adsorption measurement, aerogel was typically degassed at 85 °C for 12 h to remove solvent molecules within the network.

Synthesis of 1. Compound **2** (11.55 mmol, 4.3 g, 2 equiv) was added to a 500 mL three-neck flask with 300 mL of DCM and wrapped in a black plastic bag. Pyrrole (11.55 mmol, 812.1 μL, 2 equiv) was added into the flask; the mixture was then stirred at room temperature for 0.5 h. Then, $BF_3{\cdot}Et_2O$ (5.9 mmol, 145 mL, 1 equiv dissolved in 50 mL of DCM) was added slowly. The solution was stirred at room temperature for another 8 h. After that, DDQ (8.7 mmol, 1.97 g, 1.5 equiv) was added. The mixture was stirred for about 12 h, resulting in a solution with **3**. After removing the solvents under vacuum, the residue was purified by column chromatography (SiO_2, DCM:ethyl acetate = 25:1) to yield the desired solid compound **3** (391 mg, 20%). ^{1}H NMR (400 MHz, d_6-DMSO) δ: 9.05 (s, 8H), 8.56 (d, J = 5.9 Hz, 12H), 8.31 (s, 4H), 8.10 (t, J = 7.7 Hz, 16H), 7.69−7.47 (m, 8H), 7.26 (s, 4H), 3.90 (s, 24H). ^{13}C NMR (100 MHz, d_6-DMSO) δ: 168.2, 140.83, 139.7, 133.1, 132.5, 130.6, 129.6, 129.0. The obtained **3** (0.96 g) was stirred in a mixed solvent of THF (40 mL) and MeOH (40 mL), to which an aqueous solution of KOH (5 g of KOH in 60 mL of H_2O) was introduced. This mixture was refluxed for 3 h at 80 °C. After cooling down to room temperature, THF and MeOH were evaporated. Additional water was added to the resulting water phase until the solid was fully dissolved; then, the homogeneous solution was acidified with 1 M HCl until the solid was precipitated. The solid was collected by filtration, washed with H_2O, and dried in vacuum (0.90 g, 100%). ^{1}H NMR (400 MHz, d_6-DMSO) δ: 9.10 (s, 8H), 8.64 (s, 8H), 8.51 (d, J = 13.8 Hz, 12H), 8.35 (d, J = 7.7 Hz, 8H), 8.02 (d, J = 7.6 Hz, 8H), 7.68 (t, J = 7.7 Hz, 8H). ^{13}C NMR (100 MHz, d_6-DMSO) δ: 168.19, 143.83, 140.96, 139.73, 133.21, 133.02, 132.61, 130.48, 129.74, 129.01, 126.04, 120.57.

The Typical Procedure for Si−H Insertion. A solution of ethyl-2-diazoacetate (EDA, 45.6 mg, 0.4 mmol, 1.0 equiv) in DCM (1.0 mL) was added slowly to the mixture of silane (0.6

https://doi.org/10.1021/acsomega.1c04265
ACS Omega 2021, 6, 26766−26772

mmol, 1.5 equiv) and activated MOAs (2 mol %) in dichloromethane (DCM, 1 mL). The resulting suspension was stirred at room temperature until EDA was completely consumed. The undissolved catalyst was removed through centrifugation and washed with DCM (3 × 8 mL). The combined supernatant was evaporated to dryness, and the residue was dissolved in $CDCl_3$ and analyzed by ^1H NMR to determine the conversion of EDA.

Recycling Experiments. EDA (456 mg, 4 mmol, 1.0 equiv) was added slowly to the mixture of triethylsilane (6 mmol, 1.5 equiv) and activated MOA I (2 mol %) in DCM (10 mL). The resulting suspension was stirred at room temperature until all EDA was completely consumed. The undissolved catalyst was removed through centrifugation and washed with fresh DCM (10 mL × 4). The combined supernatant was evaporated to dryness, and the residue was dissolved in $CDCl_3$ and analyzed by ^1H NMR to determine the yield. The recycled catalyst was collected, air-dried, and then used for the successive runs.

Dyes Adsorption. The dye adsorption studies were carried out by agitating the aerogel I (8 mg) in 8 mL of dye solution (20 mg L^{-1}). The dyes were dissolved in water, respectively, and the dye concentration was determined by UV−vis spectroscopy. The wavenumbers for the UV−vis adsorption of MB, OG, and BBR-250 are 665, 481, and 588 nm, respectively.

■ ASSOCIATED CONTENT

Supporting Information

The Supporting Information is available free of charge at https://pubs.acs.org/doi/10.1021/acsomega.1c04265.

More detailed experimental procedures; ^1H NMR and ^{13}C NMR spectra of intermediates; photographs of wet gels; the FT-IR spectra of porphyrin 1 and MOA I; the TG curve of the aerogel I; the powder XRD pattern of the aerogel I; the micro- and mesoporosity distributions of the aerogels; porosity properties of aerogels A, D, I, and J; Si−H insertion of triethylsilane and EDA; Si−H insertion of EDA with different silanes (PDF)

■ AUTHOR INFORMATION

Corresponding Authors

Hong-Guang Fu − *School of Chemistry and Chemical Engineering, Qufu Normal University, Qufu 273165, P. R. China*; Email: fuhongguang1990@163.com

Jinmao You − *School of Chemistry and Chemical Engineering, Key Laboratory of Life-Organic Analysis of Shandong Province, and Key Laboratory of Pharmaceutical Intermediates and Analysis of Natural Medicine of Shandong Province, Qufu Normal University, Qufu 273165, P. R. China*; orcid.org/0000-0002-8808-6085; Email: jmyou6304@163.com

Complete contact information is available at: https://pubs.acs.org/10.1021/acsomega.1c04265

Notes

The authors declare no competing financial interest.

■ ACKNOWLEDGMENTS

We thank NNSFC (no. 21976105) and the Youth Talent Program Startup Foundation of Qufu Normal University (no. 108615001) for financial support.

■ REFERENCES

(1) Lu, H.; Li, Y.; Wang, Y.; Li, X. Preparation of $CoFe_2O_4$@Vacancy@$mSiO_2$ Core-Shell Composites for Removal of Organic Pollutant in Aqueous Solution. *J. Saudi Chem. Soc.* **2019**, *23*, 536−545.

(2) Chen, D.; Zhu, H.; Yang, S.; Li, N.; Xu, Q.; Li, H.; He, J.; Lu, J. Micro−Nanocomposites in Environmental Management. *Adv. Mater.* **2016**, *28*, 10443−10458.

(3) Zhu, Y.-H.; Yuan, S.; Bao, D.; Yin, Y.-B.; Zhong, H.-X.; Zhang, X.-B.; Yan, J.-M.; Jiang, Q. Decorating Waste Cloth via Industrial Wastewater for Tube-Type Flexible and Wearable Sodium-Ion Batteries. *Adv. Mater.* **2017**, *29*, 1603719.

(4) Wu, X.; Chen, Y.; Liu, Y. Supramolecular Crosslinked Polymer for Efficient Organic Dye Removal from Aqueous Solution. *Adv. Sustainable Syst.* **2019**, *3*, 1800165.

(5) Xu, W.; Chen, Y.; Xu, W.; Wu, X.; Liu, Y. Electrospinning Oriented Self-Cleaning Porous Crosslinking Polymer for Efficient Dyes Removal. *Adv. Mater. Interfaces* **2020**, *7*, 2001050.

(6) Huang, T.; Shao, Y.-W.; Zhang, Q.; Deng, Y.-F.; Liang, Z.-X.; Guo, F.-Z.; Li, P.-C.; Wang, Y. Chitosan-Cross-Linked Graphene Oxide/Carboxymethyl Cellulose Aerogel Globules with High Structure Stability in Liquid and Extremely High Adsorption Ability. *ACS Sustainable Chem. Eng.* **2019**, *7*, 8775−8788.

(7) Gong, Y.; Chen, Z.; Bi, L.; Kang, J.; Zhang, X.; Zhao, S.; Wu, Y.; Tong, Y.; Shen, J. Adsorption Property and Mechanism of Polyacrylate-Divinylbenzene Microspheres for Removal of Trace Organic Micropollutants from Water. *Sci. Total Environ.* **2021**, *781*, 146635.

(8) Hui, M.; Shengyan, P.; Yaqi, H.; Rongxin, Z.; Anatoly, Z.; Wei, C. A Highly Efficient Magnetic Chitosan "Fluid" Adsorbent with a High Capacity and Fast Adsorption Kinetics for Dyeing Wastewater Purification. *Chem. Eng. J.* **2018**, *345*, 556−565.

(9) Momina; Ahmad, K. Study of Different Polymer Nanocomposites and Their Pollutant Removal Efficiency: Review. *Polymer* **2021**, *217*, 123453.

(10) Saraji, M.; Shahvar, A. Metal-Organic Aerogel as a Coating for Solid-Phase Microextraction. *Anal. Chim. Acta* **2017**, *973*, 51−58.

(11) Vellingiri, K.; Deng, Y.-X.; Kim, K.-H.; Jiang, J.-J.; Kim, T.; Shang, J.; Ahn, W.-S.; Kukkar, D.; Boukhvalov, D. W. Amine-Functionalized Metal−Organic Frameworks and Covalent Organic Polymers as Potential Sorbents for Removal of Formaldehyde in Aqueous Phase: Experimental Versus Theoretical Study. *ACS Appl. Mater. Interfaces* **2019**, *11*, 1426−1439.

(12) Keum, Y.; Kim, B.; Byun, A.; Park, J. Synthesis and Photocatalytic Properties of Titanium-Porphyrinic Aerogels. *Angew. Chem., Int. Ed.* **2020**, *59*, 21591−21596.

(13) Kandambeth, S.; Dey, K.; Banerjee, R. Covalent Organic Frameworks: Chemistry beyond the Structure. *J. Am. Chem. Soc.* **2019**, *141*, 1807−1822.

(14) (a) Vallejo-Sánchez, D.; Amo-Ochoa, P.; Beobide, G.; Castillo, O.; Fröba, M.; Hoffmann, F.; Luque, A.; Ocón, P.; Pérez-Yáñez, S. Chemically Resistant, Shapeable, and Conducting Metal-Organic Gels and Aerogels Built from Dithiooxamidato Ligand. *Adv. Funct. Mater.* **2017**, *27*, 1605448. (b) Zhao, J.; Yan, X. Rh(II)-based Metal−Organic Polyhedra. *Chem. Lett.* **2020**, *49*, 659−665. (c) Gui, B.; Meng, Y.; Xie, Y.; Du, K.; Sue, A. C.-H.; Wang, C. Immobilizing Organic-Based Molecular Switches into Metal−Organic Frameworks: A Promising Strategy for Switching in Solid State. *Macromol. Rapid Commun.* **2018**, *39*, 1700388.

(15) Wang, Z.; Zhang, J.-H.; Jiang, J.-J.; Wang, H.-P.; Wei, Z.-W.; Zhu, X.; Pan, M.; Su, C.-Y. A Stable Metal Cluster-Metalloporphyrin MOF with High Capacity for Cationic Dye Removal. *J. Mater. Chem. A* **2018**, *6*, 17698−17705.

(16) Akhtar, F.; Andersson, L.; Ogunwumi, S.; Hedin, N.; Bergström, L. Structuring Adsorbents and Catalysts by Processing of Porous Powders. *J. Eur. Ceram. Soc.* **2014**, *34*, 1643−1666.

(17) Zhang, J.; Su, C.-Y. Metal-organic gels: From Discrete Metallogelators to Coordination Polymers. *Coord. Chem. Rev.* **2013**, *257*, 1373−1408.

(18) Nune, S. K.; Thallapally, P. K.; McGrail, B. P. Metal Organic Gels (MOGs): a New Class of Sorbents for CO_2 Separation Applications. *J. Mater. Chem.* **2010**, *20*, 7623−7625.
(19) Wei, S.-C.; Pan, M.; Li, K.; Wang, S.; Zhang, J.; Su, C.-Y. A Multistimuli-Responsive Photochromic Metal-Organic Gel. *Adv. Mater.* **2014**, *26*, 2072−2077.
(20) Fu, H.-G.; Chen, Y.; Liu, Y. Multistimuli-Responsive and Photocontrolled Supramolecular Luminescent Gels Constructed by Anthracene-Bridged Bis(dibenzo-24-crown-8) with Secondary Ammonium Salt Polymer. *ACS Appl. Mater. Interfaces* **2019**, *11*, 16117−16122.
(21) Liao, P.; Cai, G.; Shi, J.; Zhang, J. Post-Modified Porphyrin Imine Gels with Improved Chemical Stability and Efficient Heterogeneous Activity in CO_2 Transformation. *New J. Chem.* **2019**, *43*, 10017−10024.
(22) Li, L.; Xiang, S.; Cao, S.; Zhang, J.; Ouyang, G.; Chen, L.; Su, C.-Y. A Synthetic Route to Ultralight Hierarchically Micro/Mesoporous Al(III)-Carboxylate Metal-Organic Aerogels. *Nat. Commun.* **2013**, 1774.
(23) Farha, O. K.; Özgür Yazaydın, A.; Eryazici, I.; Malliakas, C. D.; Hauser, B. G.; Kanatzidis, M. G.; Nguyen, S. T.; Snurr, R. Q.; De Hupp, J. T. Novo Synthesis of A Metal−Organic Framework Material Featuring Ultrahigh Surface Area and Gas Storage Capacities. *Nat. Chem.* **2010**, *2*, 944−948.
(24) Furukawa, H.; Ko, N.; Go, Y. B.; Aratani, N.; Choi, S. B.; Choi, E.; Yazaydin, A. Ö.; Snurr, R. Q.; O'Keeffe, M.; Kim, J.; Yaghi, O. M. Ultrahigh Porosity in Metal-Organic Frameworks. *Science* **2010**, *329*, 424.
(25) Saito, S.; Osuka, A. Expanded Porphyrins: Intriguing Structures, Electronic Properties, and Reactivities. *Angew. Chem., Int. Ed.* **2011**, *50*, 4342−4373.
(26) Bagheri, V.; Doyle, M. P.; Taunton, J.; Claxton, E. E. A New and General Synthesis of Alpha.-Silyl Carbonyl Compounds by Silicon-Hydrogen Insertion from Transition Metal-Catalyzed Reactions of Diazo Esters and Diazo Ketones. *J. Org. Chem.* **1988**, *53*, 6158−6160.
(27) Huang, M.-Y.; Yang, J.-M.; Zhao, Y.-T.; Zhu, S.-F. Rhodium-Catalyzed Si−H Bond Insertion Reactions Using Functionalized Alkynes as Carbene Precursors. *ACS Catal.* **2019**, *9*, 5353−5357.
(28) Kang, J.; Zhu, B.; Liu, J.; Wang, B.; Zhang, L.; Su, C.-Y. Chiral Dirhodium Catalysts Derived from L-serine, L-threonine and L-cysteine: Design, Synthesis and Application. *Org. Chem. Front.* **2015**, *2*, 890−907.
(29) Johnson, J. A.; Lin, Q.; Wu, L.-C.; Obaidi, N.; Olson, Z. L.; Reeson, T. C.; Chen, Y.-S.; Zhang, J. A "Pillar-Free," Highly Porous Metalloporphyrinic Framework Exhibiting Eclipsed Porphyrin Arrays. *Chem.Commun.* **2013**, *49*, 2828−2830.

https://doi.org/10.1021/acsomega.1c04265
ACS Omega 2021, 6, 26766−26772